

Small gold clusters on graphene, their mobility and clustering: A DFT study

Martin Amft,* Biplab Sanyal, Olle Eriksson, and Natalia V. Skorodumova

Department of Physics and Astronomy, Uppsala University, Box 516, S-751 20 Uppsala, Sweden

(Dated: October 11, 2010)

Motivated by the experimentally observed high mobility of gold atoms on graphene and their tendency to form nanometer-sized clusters, we present a density functional theory study of the ground state structures of small gold clusters on graphene, their mobility and clustering. Our detailed analysis of the electronic structures identifies the opportunity to form strong gold-gold bonds and the graphene mediated interaction of the pre-adsorbed fragments as the driving forces behind gold's tendency to aggregate on graphene. While clusters containing up to three gold atoms have one unambiguous ground state structure, both gas phase isomers of a cluster with four gold atoms can be found on graphene. In the gas phase the diamond shaped Au_4^D cluster is the ground state structure, whereas the Y shaped Au_4^Y becomes the actual ground state when adsorbed on graphene. As we show, both clusters can be produced on graphene by two distinct clustering processes. We also studied in detail the stepwise formation of a gold dimer out of two pre-adsorbed adatoms, as well as the formation of Au_3 . All reactions are exothermic and no further activation barriers, apart from the diffusion barriers, were found. The diffusion barriers of all studied clusters range from 4 to 36 meV, only, and are substantially exceeded by the adsorption energies of -0.1 to -0.59 eV. This explains the high mobility of Au_{1-4} on graphene along the C-C bonds.

PACS numbers: 71.15.Nc, 78.67.Bf, 68.43.Fg

I. INTRODUCTION

Historically, carbon allotropes, e.g. graphite, carbon nanotubes, and fullerene have been extensively used for studying the absorption processes of finite-sized particles on them. Small coinage metal clusters on single layers of carbon, i.e. graphene, were first used to model the adsorption on graphite surfaces or single-walled carbon nanotubes.¹⁻³ After the experimental evidence for the existence of graphene was found by Novoselov et al.^{4,5}, now even awarded with the Nobel Prize in Physics, the study of cluster adsorption on graphene became important in its own right.

Graphene stands as an extraordinary material that offers enormous possibilities for applications in electronics, sensors, biodevices, catalysis, and energy storage.⁶⁻⁹ The unique electronic structure of graphene with a linear dispersion of the electronic structure at Dirac points not only plays an important role in charge transport but in verifying theoretical predictions in quantum electrodynamics by table-top experiments, too. As graphene is a zero band gap material, one of the routes to make use of graphene in electronics industry is to create a small band gap by means of functionalization with external chemical agents.¹⁰⁻¹²

By means of density functional theory, the effect of Au nanoparticles on the electronic structure of graphene has been studied.¹³ The authors showed that Au_{38} nanoparticles covered with methylthiolate molecules introduce new Dirac-type points due to charge transfer but keeping the graphene layer metallic whereas the bare nanoparticle opens up a small band gap at the Dirac point of graphene. A recent work¹⁴ has emphasized the effects of the distribution of Au atoms on the charge carrier mobility of graphene. They have concluded that the formation

of Au clusters increases the mobility whereas a homogeneous distribution reduces the mobility.

The adsorption and diffusion of gold adatoms on highly oriented pyrolytic graphite (HOPG) have been studied for decades, first, by means of the desorption flux from the surface¹⁵, later on directly with scanning tunneling microscopy¹⁶, and transmission electron microscopy.¹⁷ Also *ab-initio* calculations on the adsorption of small gold clusters and the diffusion of adatoms and dimers on HOPG have been reported.¹⁸⁻²⁰

Very recently the growth of gold nanoparticles on few layers of graphene by physical vapor deposition has been monitored.²¹ The growth process stopped at an average particle size of 6.46 ± 0.68 nm on a single graphene sheet. As atomic-scale manipulation is nowadays possible in experiments, the study of small clusters and their effects on the electronic properties is highly relevant for the future realizations of nanoscale devices.

A systematic theoretical study of the size variation of small Au clusters adsorbed on graphene is missing. Here we address this issue by means of density functional theory (DFT). We study the adsorption of Au_{1-4} on graphene, focusing on an analysis of the electronic structures. Diffusion barriers are calculated from the total energies and confirm the high mobility of Au_{1-4} . We study in detail the step-wise formation of a gold dimer out of two pre-adsorbed adatoms, as well as the formation of $\text{Au}_{3,4}$. We show how both Au_4 isomers from the gas phase can be produced on graphene by two distinct clustering processes.

This paper is organized as follows. In the next section II we summarize the computational details of this work. In Sec. III the ground state structures of Au_{1-4} /graphene, their adsorption energies, charge transfers, and electronic structures are discussed. Starting from these structures the mobility, i.e. diffusion barriers

ers, and clustering processes have been studied and are presented in Sec. IV. Finally, Sec. V summarizes and concludes the paper.

II. COMPUTATIONAL DETAILS

The scalar-relativistic *ab-initio* DFT calculations were performed using the projector augmented wave (PAW)^{22,23} method as implemented in VASP.^{24,25} The exchange-correlation interaction was treated in the generalized gradient approximation (GGA) in the parameterization of Perdew, Burke, and Ernzerhof (PBE).²⁶ A cut-off energy of 600 eV was used and a Gaussian smearing with a width of $\sigma = 0.05$ eV for the occupation of the electronic levels. Spin-polarization was taken into account for all calculations.

The graphene sheet was modeled by a 5×5 supercell, i.e. 50 carbon atoms, using the calculated C-C bond length of 1.42 Å. The repeated sheets were separated from each other by 20 Å of vacuum. A Monkhorst-Pack Γ -centered $5 \times 5 \times 1$ k-point mesh (13 k-points in the irreducible wedge of the Brillouin-Zone) was used for the structural relaxations. The relaxation cycle was stopped when the Hellman-Feynman forces had become smaller than $5 \cdot 10^{-3}$ eV/Å. We also used a finer k-point mesh, i.e. $16 \times 16 \times 1$ k-point mesh (130 k-points) and found the changes in the geometry of the systems to be negligible. Therefore we decided to use the relaxed structures obtained with the $5 \times 5 \times 1$ k-point mesh for total energy (E_0) and density of states (DOS) calculations. However we used a finer k-point mesh, i.e. $20 \times 20 \times 1$ with 202 k-points, to accurately calculate E_0 and the DOS of these structures. Note that cluster adsorption energies, $E_{\text{ads}} = E_0(\text{Au}_{1-4}/\text{graphene}) - E_0(\text{Au}_{1-4}) - E_0(\text{graphene})$, are negative when the adsorption is exothermic. The projected DOS were calculated within Wigner-Seitz spheres of radii 0.863 Å (carbon) and 1.503 Å (gold), using for illustrative purposes a higher Gaussian smearing of 0.1 eV.

In order to obtain the diffusion barriers the total energies of the gold clusters on different binding sites were calculated. In the calculations the x-y coordinates of the gold atom binding to carbon, as well as the carbon atoms in the rim, were fixed, while the rest of the structure could fully relax. Since the calculated diffusion barriers are less than 36 meV, we checked their dependence on the used GGA exchange-correlation functional. Compared to PW91²⁷ and RPBE²⁸, we found negligible differences only.

The charge distributions and transfers were analyzed by means of the Bader analysis.²⁹

III. GROUND STATE PROPERTIES OF $\text{Au}_{1-4}/\text{GRAPHENE}$

There are different ways to obtain clusters of a certain size on a substrate. Here we consider two possibilities: first, mass selected clusters soft-landed onto graphene and, second, the clustering of smaller fragments, already pre-adsorbed on the graphene sheet.

When exploring the first scenario, we obtain the ground state structures of $\text{Au}_{1-4}/\text{graphene}$, see Fig. 1 (a)-(d), by fully relaxing the gas phase cluster ground state structures³⁰⁻³² in various ways on graphene. As will be shown in Sec. IV, the same structures for Au_{2-4} are formed when starting from smaller pre-adsorbed fragments, i.e. by the second scenario.

The tetramer shows an interesting peculiarity. In the gas phase the diamond shaped isomer, Au_4^D , is the ground state.³⁰⁻³² According to our calculations, it is 43 meV lower in energy than the Y shaped isomer, Au_4^Y , cf. Refs [30,32]. On graphene the situation is reversed: $\text{Au}_4^Y/\text{graphene}$ is 137 meV lower in energy than $\text{Au}_4^D/\text{graphene}$. The overall geometry of both isomers is conserved on graphene, cf. Fig. 1 (d) and (e). In addition to soft-landing, both isomers can be formed on graphene by clustering of smaller pre-adsorbed fragments, i.e. $\text{Au}_1 + \text{Au}_3 \rightarrow \text{Au}_4^D$ and $2 \cdot \text{Au}_2 \rightarrow \text{Au}_4^Y$, see Sec. IV for more details. Note that two of the bonds in Au_4^Y are comparable to the inter-dimer bond, i.e. 2.55 and 2.6 Å compared to 2.67 and 2.72 Å, cf. Figs 1 (b) and (e).

A. Binding sites and energies, charge redistribution

The adatom, dimer, and Y shaped tetramer prefer the binding site on top of a carbon atom, whereas the trimer and diamond shaped tetramer bind right above a carbon-carbon bond, see Fig. 1 for an illustration. It is interesting to observe a trend to minimize the number of gold atoms binding to graphene for all five clusters, i.e. only one Au atom is close to the graphene layer. This already indicates that the Au-Au interaction is stronger than Au-C interaction, which will be discussed in greater detail below.

The ground state structures of $\text{Au}_{1,2}/\text{graphene}$, see Fig. 1 (a) and (b), resemble the adsorption behavior of $\text{Au}_{1,2}$ on MgO and graphite.^{18,33,34} The adsorption behavior of the trimer and tetramers on graphene, Figs 1 (c)-(e), is in contrast to the adsorption of small gold clusters on MgO terraces. On MgO the gold trimer and tetramer form two bonds between gold and surface oxygen. Furthermore only the diamond shaped Au_4 isomer is stable on that substrate.³³

Care must be taken when comparing our results with earlier studies of Au_{1-4} on HOPG.¹⁸⁻²⁰ First of all the authors relied on the use of the local density approximation (LDA), which only coincidentally describes the bulk properties of graphite better than GGA. Secondly, the number of k-points was eight at best, making a meaning-

ful calculation of, for instance, the DOS impossible. Last but not least, spin-polarization was neglected in Refs [18,20]. We find spin-polarization especially important for open shell systems like $\text{Au}_{1,3}/\text{graphene}$. They have two distinct peaks, for spin up and down states, respectively, close to the Fermi level, cf. Figs 4 and 5. Albeit all these methodological differences one can conclude that the ground state structures of Au_{1-3} adsorbed on HOPG and graphene seem to be very similar. Note that $\text{Au}_{3,4}$ have not been studied on graphene before. The second isomer, Au_4^Y Fig. 1 (e), has not even been considered on graphite before. Note that the tetrahedral structure of Au_4 is known to be unstable in the gas phase^{32,35} and neither did we find this structure on graphene.

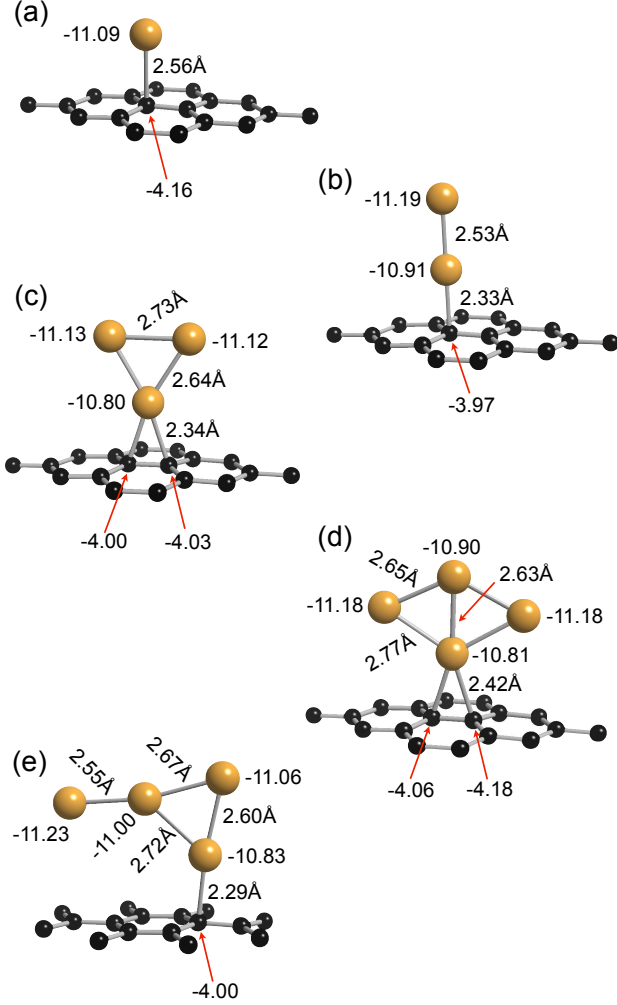


FIG. 1: (Color online) Ground state structures of Au_{1-4} on a 5×5 graphene sheet. Structures (a)-(d) were obtained by soft-landing the clusters from the gas phase. The isomer Au_4^Y (e) is formed by clustering two pre-adsorbed dimers. It is 137 meV lower in energy than $\text{Au}_4^D/\text{graphene}$ (d). Also given are relevant bond lengths and Bader charges. Note: in our calculations neutral Au atoms have a Bader charge of -11 and C atoms of -4, respectively.

Figure 2 (a) shows the cluster adsorption energies E_{ads}

of the Au_{1-3} ground state structures, as well as of both Au_4 isomers. Au_4^Y has the highest E_{ads} of -0.59 eV and the adatom having with -0.1 eV the lowest. As mentioned above, Au_4^Y is not only the ground state structure on graphene, but also adsorbs stronger on it than Au_4^D , i.e. $E_{\text{ads}} = -0.59$ vs. -0.41 eV, respectively.

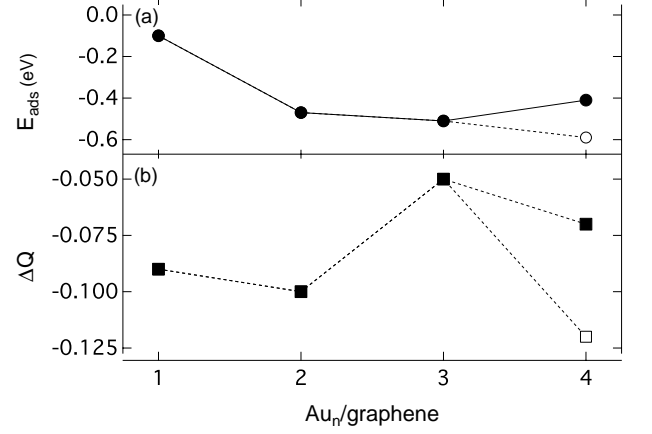


FIG. 2: (Color online) Upper panel (a): Cluster adsorption energy of Au_{1-4} on graphene. Lower panel (b): total charge transferred from the graphene sheet into the clusters, calculated by the Bader analysis. Full symbols: gas phase structures adsorbed on graphene, cf. Figs 1 (a) - (d). Open symbols: Y shaped $\text{Au}_4^Y/\text{graphene}$, cf. Fig. 1 (e).

In all the five cases the whole gold cluster receives, according to our Bader analysis, a small charge of up to $-0.12 e^-$ from graphene, see Fig. 2 (b). Hence adsorbing Au_{1-4} on graphene corresponds to a p-doping of the material. A clear odd-even oscillation, depending on the number of gold atoms in the cluster, can be seen in the charge transfer. It is generally known that the electronic characteristics of low-dimensional gold structures can exhibit odd/even oscillations depending on the parity of the number of Au atoms, which are determined by the opening/closing of the s -shell.^{33,36,37}

In addition to the charge transfer into the clusters, there occurs also a significant charge redistribution within the clusters themselves, see Bader charges of the individual atoms in Fig. 1. The insets in Figs 4 - 8 also illustrate it by showing isosurfaces of the charge density redistribution, i.e. $\Delta\rho = \rho(\text{Au}_n/\text{graphene}) - \rho(\text{Au}_n) - \rho(\text{graphene})$, upon the cluster adsorption on graphene. In the case of Au_{2-4} up to 0.19 electrons are redistributed from the gold atom binding to graphene into the rest of the cluster.

Concerning the adsorption strength of these small gold clusters on graphene we can summarize that two effects exist, which can compete with each other. First, the attraction due to the formation of chemical bonds between gold and carbon. Second, there also exists a Coulomb interaction between the charged gold atoms in the cluster and the carbon atoms in the proximity of the adsorption site. Mostly this Coulomb interaction is repulsive

in nature, as it can be seen from the extra charge in the clusters that tends to be concentrated as far away from the graphene sheet as possible, see Figs 1 (a) - (c).

Although the extra charge density concentrates on the two outer atoms in $\text{Au}_4^D/\text{graphene}$, those two atoms are repelled away from the graphene sheet, recognizable from the 5% stretched bonds with the bottom gold atom, see Fig. 1 (d). In contrast to these four systems, the Coulomb interaction between the adsorbed Au_4^Y and the underlying graphene sheet is predominately attractive, i.e. between the left-most gold atom, cf. Fig. 1 (e), carrying most of the additional charge, and the positively charged carbon atoms under it, cf. inset in Fig. 7.

The comparatively small adsorption energy of the single gold atom is also explained by these competing effects, see Fig. 1 (a), which is manifested in the 5-9 % longer Au-C distance of $\text{Au}_1/\text{graphene}$ compared to the other clusters.

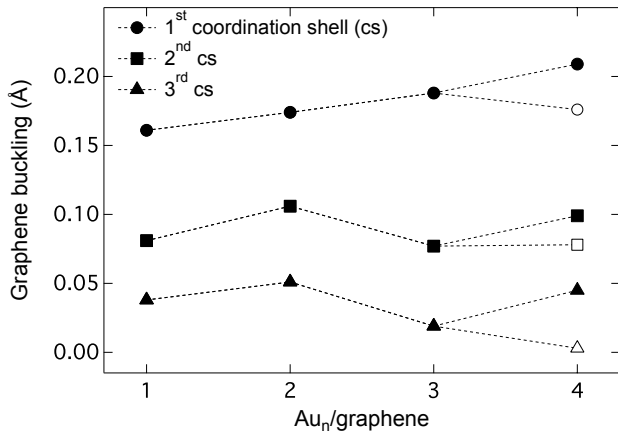


FIG. 3: (Color online) Buckling, i.e. vertical distortion, of the first three coordination shells around the adsorption sites of Au_{1-4} . Full symbols: gas phase structures adsorbed on graphene, cf. Figs 1 (a) - (d). Open symbols: $\text{Au}_4^Y/\text{graphene}$, cf. Fig. 1 (e).

It has, predominantly qualitatively, been reported in the literature that the adsorption of Au_{1-4} on HOPG^{18-20,38} and of $\text{Au}_{1,2}$ on graphene^{39,40} leads to a shift of the carbon atoms in the vicinity of the adsorption site towards the gold. Due to the strong sp^2 interatomic C-C bonds the vertical distortion is not solely restricted to the carbon atoms underneath gold. Instead it spreads at least to the third coordination shell around the adsorbate, cf. Fig. 3. Lets consider for the moment only the gas phase structures adsorbed on graphene. The full symbols in Fig. 3 show that the vertical distortion of the carbon atoms binding to the Au atom scales approximately linear with the size of the gold cluster. On the other hand, the buckling in the second and third coordination shell does show a clear odd-even oscillation depending on the number of Au atoms, Fig. 3 (full symbols). But the actual tetramer ground state geometry $\text{Au}_4^Y/\text{graphene}$ breaks these trends, showing a significantly smaller dis-

tortion of the C atom positions than $\text{Au}_4^D/\text{graphene}$, see Fig. 3 (open symbols).

Along with the buckling comes a polarization of the graphene sheet, i.e. charge deviations from otherwise neutral charge state of the carbon atoms, of up to $\pm 0.18 e^-$. For the systems under consideration the polarization does not show such a clear pattern as observed on HOPG.^{18,20} For instance, the carbon atom binding to $\text{Au}_{1,3}$ and Au_4^D gain additional electrons, whereas it stays neutral when binding to Au_4^Y or even loses some charge as under Au_2 . Also in the second and third coordination shells around the binding sites a general pattern could not be observed, i.e. charge losses and gains could be observed within the same coordination shell.

B. Electronic structure of $\text{Au}_{1,3}/\text{graphene}$

Both the gold adatom and trimer possess an unpaired 6s electron that gives rise to a total spin moment of $1\mu_B$ in the system.

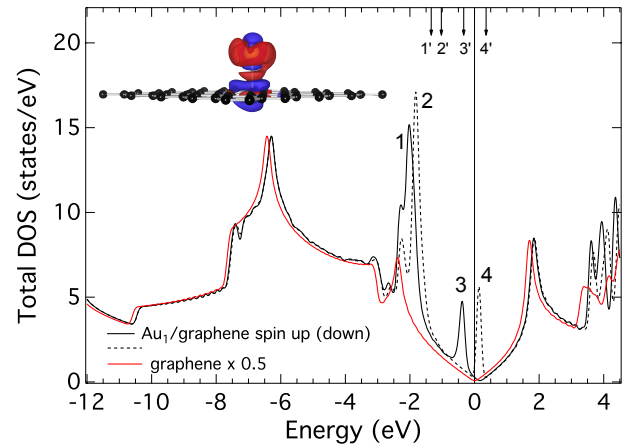


FIG. 4: (Color online) Projected spin-polarized total DOS of $\text{Au}_1/\text{graphene}$ (black lines; solid spin up; dashed spin down) and for comparison pure graphene (red line). Note: the Fermi energies of both systems were shifted to 0 eV. Inset: charge density redistribution due to adsorption of Au_1 on graphene; increase (decrease) of the charge density in red (blue). The shown isosurfaces correspond to $\pm 7 \cdot 10^{-4} e^-/\text{\AA}^3$. The arrows on the top show the atomic energy levels of a single gold atoms.

Figures 4 and 5 show the total spin-polarized DOS of $\text{Au}_{1,3}/\text{graphene}$ and, for comparison, also the total DOS of pure graphene. For illustration the atomic energy levels of an isolated gold atom are shown as arrows in Fig. 4. Only in this simple case the origin of the electronic states of the adsorbed adatom can easily be identified from the gas phase species.

From the lm and site decomposed DOS (not shown) we identified the character of the labeled structures 1-4 in the DOS of $\text{Au}_1/\text{graphene}$ and accordingly for the bigger clusters as well.

In Fig. 4 the structures no. 1 (2) are gold 5d-states with spin polarization up (down). The higher peaks in 1 and 2 consist partially of d_{z^2} -states that overlap with p_z -states of the underlying carbon atom. Also the gold 6s-state near the Fermi level, i.e. peak 3, hybridizes with the p_z -state to form a σ -bond. The unoccupied states in peak 4 are of similar character as those in no. 3. Compared to the atomic states, i.e. arrows 1' and 2' in Fig. 4, the d -states are split upon adsorption of the gold atom on graphene. Furthermore they are shifted approximately 0.7 eV downwards in energy. The gap between the highest occupied states and the lowest unoccupied states ΔE_G , i.e. between the peaks 3 and 4, is 0.15 eV narrower than in the gas phase, i.e. 3' and 4'.

For the bigger clusters, we concentrate our efforts on the identification of the most important features of the densities of states, i.e. Figs 5 - 8, and their contribution to the formation of the clusters and their bonding to graphene.

Already at a first glance at the DOS of $\text{Au}_3/\text{graphene}$, Fig. 5, one can recognize the higher complexity of the structure. The two peaks labeled with 1 comprise predominantly of d_{yz} and $d_{x^2-y^2}$ -states of the gold atom closest to carbon, hybridizing with its p -states. The peaks no. 2 are predominantly $d_{x^2-y^2}$ -states located at the two gold atoms at the top. The main features, no. 3, mostly contain d -states of all characters from the top gold atoms. Most of the d_{z^2} -states of all three gold atoms are concentrated in this peak, forming the chemical bond to carbon by hybridizing with its p_z -states. Peak no. 4 consists of intracluster d_{xz} - d_{z^2} states. The peak no. 5 directly below the Fermi energy contains the 6s-states of the top gold atoms that interact only indirectly, via d_{xz} -states of the gold atom closest to graphene, with the carbon p_z -states. Clearly, most of the spin-moment of the whole system is concentrated in these states. Finally, the peaks 6 and 7 in the unoccupied DOS are overlaps of empty 6s-states and carbon p_z -states from the top gold atoms and the bottom one, respectively.

From the shown DOS, especially the peaks near the Fermi energy, one can conclude that even a small external bias of less than ± 0.5 V will significantly increase the electrical conductivity of these systems.

The charge density redistributions upon adsorption $\Delta\rho$ are shown as insets in Figs 4 and 5. The earlier mentioned polarization of the carbon atoms in the first three coordination shells around the adsorption sites can be seen. The extra charge in Au_1 also leads to a charge density redistribution within the gold atom, whereas the gold atoms in the trimer seem to equally share the additional charge from the substrate. Therefore it is important to take the Bader analysis, Fig. 1, into consideration as well that showed a charge depletion of the bottom gold atom.

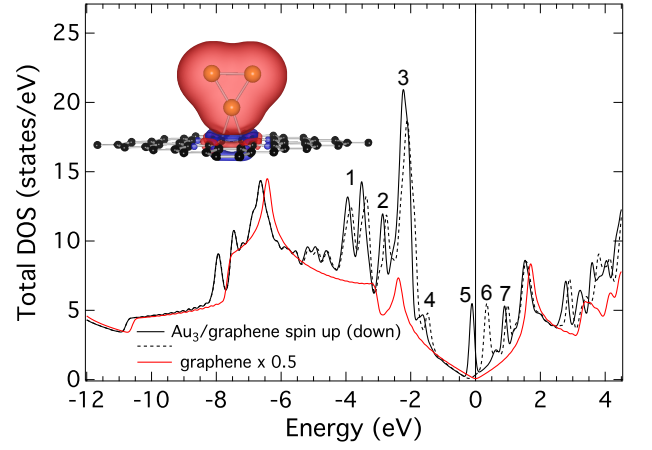


FIG. 5: (Color online) Projected spin-polarized total DOS of $\text{Au}_3/\text{graphene}$ (black lines; solid spin up; dashed spin down) and for comparison pure graphene (red line). Note: the Fermi energies of both systems were shifted to 0 eV. Inset: charge density redistribution due to adsorption of Au_3 on graphene; increase (decrease) of the charge density in red (blue). The shown isosurfaces correspond to $\pm 7 \cdot 10^{-4} \text{ e}^-/\text{\AA}^3$.

C. Electronic structure of $\text{Au}_{2,4}/\text{graphene}$

Obviously, the total magnetic moment of the closed shell structures $\text{Au}_{2,4}$ must be zero in the gas phase. This is unchanged by adsorbing them on graphene.

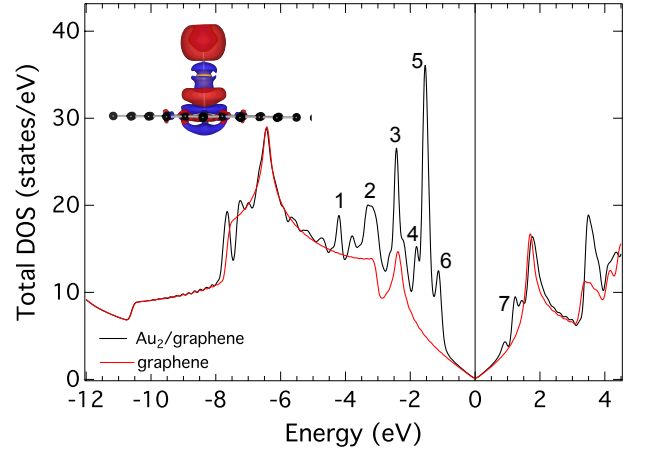


FIG. 6: (Color online) Projected total DOS of $\text{Au}_2/\text{graphene}$ (black line) and for comparison pure graphene (red line). Note: the Fermi energies of both systems were shifted to 0 eV. Inset: charge density redistribution due to adsorption of Au_2 on graphene; increase (decrease) of the charge density in red (blue). The shown isosurfaces correspond to $\pm 7 \cdot 10^{-4} \text{ e}^-/\text{\AA}^3$.

Upon adsorption the symmetry of the electronic structure of the dimer is broken, see Fig. 6. From the lm and site decomposed DOS (not shown), we see that peak no. 1 consists of d_{z^2} -states. The broader feature no. 2 and peak no. 3 are d_{xy} , d_{yz} , and $d_{x^2-y^2}$ -states, predomi-

nantly from the gold atom closest to carbon, hybridizing with carbon $p_{x,y}$ -states. Peaks 4 and 5 do not contribute to the chemical bonding to graphene, as they are s - d -states localized at the cluster. Whereas no. 6, mostly s - d_{z^2} -states at the top gold atom, indirectly interacts with carbon p_z via d_{z^2} at the bottom gold atom. Finally, the two peaks at no. 7 are predominantly unoccupied $6s$ -states of the gold atom close to carbon, overlapping empty p_z -states of carbon. Note also that the states in peaks 4-7 substantially narrow the cone in graphene's DOS around the Fermi energy, leaving it only undisturbed in the interval $E_F \pm 0.5$ eV, Fig. 6.

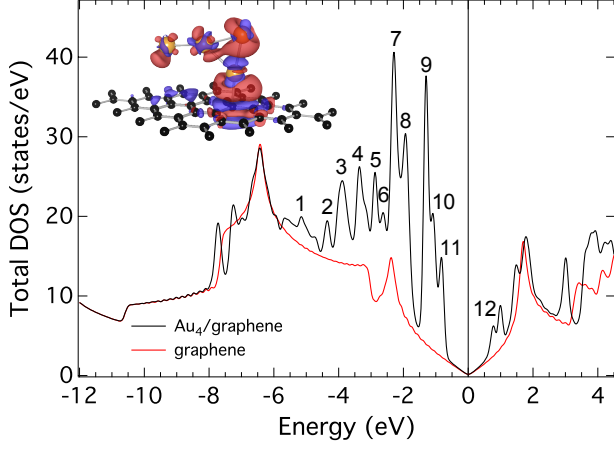


FIG. 7: (Color online) Projected total DOS of the Y shaped Au_4 /graphene (black line), see Fig. 1 (e), and for comparison pure graphene (red line). Note: the Fermi energies of both systems were shifted to 0 eV. Inset: charge density redistribution due to adsorption of Au_4 on graphene; increase (decrease) of the charge density in red (blue). The shown isosurfaces correspond to $\pm 7 \cdot 10^{-4} \text{ e}^-/\text{\AA}^3$.

To summarize the predominant nature of the labeled peaks in the DOS of Au_4^Y /graphene, Fig. 7, we label the gold atoms in the following way, see Fig. 1 (e): Au^l (left), Au^m (middle), Au^t (top), and Au^b (bottom). The carbon atom under Au^b , forming the chemical bond with the cluster, is named C^b .

Peaks no. 1 and 2 consist of s - d -states, d_{z^2} -states respectively, localized on the cluster only. Peak no. 3 consists of d -states that contribute to the chemical bond by overlapping with p_y -states of C^b , i.e. d_{xz} -states on Au^m and d_{yz} -states on $\text{Au}^{t,b}$. The peak no. 4 and its shoulder consist mainly of d_{xy} and $d_{x^2-y^2}$ on Au^b overlapping with carbon p -states as well. Peak no. 5 are $d_{x^2-y^2}$ -states solely localized within the cluster, while no. 6 are s - d_{z^2} -states of Au^b hybridizing strongly with p_z of C^b . The highest peak no. 7 consists of d_{xy} and $d_{x^2-y^2}$ -states of Au^l , Au^m , and Au^t , i.e. a major part of the strong gold-gold bonds that hold the cluster together. Peaks no. 8 and 9 are d -states almost exclusively localized on Au^m and Au^l , respectively, as well as peaks no. 10 ($d_{x^2-y^2}$ -states) and 11 (s - d_{xy} -states) which are localized on Au^l . As we saw for the other clusters the unoccupied states at

peak no. 12 are s -states, in the present case of Au^t and Au^b , overlapping with unoccupied p_z -states of C^b .

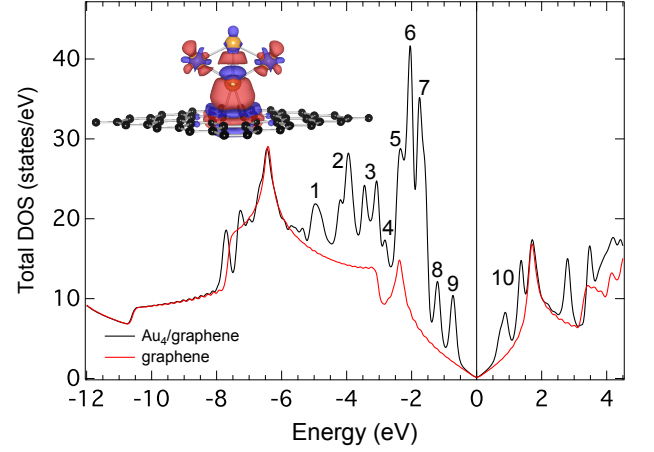


FIG. 8: (Color online) Projected total DOS of the diamond shaped Au_4 /graphene (black line), see Fig. 1 (e), and for comparison pure graphene (red line). Note: the Fermi energies of both systems were shifted to 0 eV. Inset: charge density redistribution due to adsorption of Au_4 on graphene; increase (decrease) of the charge density in red (blue). The shown isosurfaces correspond to $\pm 7 \cdot 10^{-4} \text{ e}^-/\text{\AA}^3$.

Despite its more symmetric geometry the DOS of Au_4^D /graphene, Fig. 8, has many features which can be recognized from the other isomer, cf. Fig. 7. For convenience we label the gold atoms in Au_4^D /graphene again: Au^b (bottom), Au^m (middle), and Au^t (top), see Fig. 1 (d). The two carbon atoms, forming bonds with the cluster, have a very similar electronic structure and we therefore simply name them both C^b .

The relatively broad peak no. 1 consists mainly of d_{xz} -states of Au^b and Au^t . The shoulder below peak no. 2, are d_{z^2} - d_{xy} -cluster states of Au^b and Au^t , with a smaller amount of intermixed s -states that hybridize with the p -states of C^b . The actual peak no. 2 and the double-peak no. 3 are predominantly d_{yz} and $d_{x^2-y^2}$ -states of Au^b and Au^t , respectively. The lower peak no. 4 contains s - d_{xy} -states of Au^b that also overlap with C^b p_z -states. The high peaks no. 5 to 7 are the strong intracluster bonds, formed out of d -states. Peak no. 8 on the other hand consists mainly of d_{xz} -states of Au^m , as well as d_{z^2} -states of Au^t and Au^b , contributing to the chemical bond to carbon by hybridizing with p_z -states of C^b . The highest occupied states, peak no. 9, are again intracluster bonds, formed out of s -states of the Au^m and d_{xz} -states of Au^t and Au^b . As for the other clusters the lowest unoccupied states, peaks no. 10, are unoccupied s -states on all the four gold atoms, that overlap with unoccupied C^b p_z -states.

The gap between the highest occupied states and the lowest unoccupied cluster states ΔE_G in Fig. 7 and 8 is very similar, but smaller than that in the dimer case, Fig. 6. Hence, in contrast to $\text{Au}_{1,3}$ /graphene, an external bias of more than ± 0.5 V is needed to see a significant

increase in the electrical conductivity.

IV. MOBILITY AND CLUSTERING

In this section we discuss the mobility and initial clustering processes of gold on graphene. First experiments on the diffusion and desorption of gold atoms on graphite date almost three decades back.¹⁵ With the rise of STM's quantitative estimates of the diffusion and desorption barriers became feasible. These experiments revealed that the binding energies of $\text{Au}_{1,2}$ on graphite exceed their diffusion barriers.¹⁶ Computations of gold adatoms and dimers on HOPG supported these experiments.¹⁹

A. Diffusion along the C-C bonds

We determined the diffusion barriers for Au_{1-4} on graphene from the total energies on the top (t) and bridge (b) positions, as well as from one position in between those two (tb). These energies are sufficient, since none of the five clusters was found to bind to graphene at the hollow sites, i.e. in the center of a carbon hexagon.

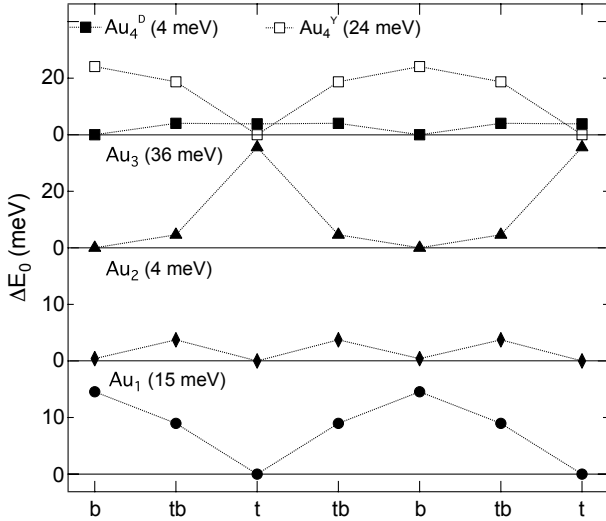


FIG. 9: (Color online) Difference in the total energies ΔE_0 at the top (t), bridge (b), and a positions in between (tb) of Au_{1-3} and $\text{Au}_4^{Y,D}$ on graphene. E_0 of the respective cluster ground state was subtracted to show the diffusion barriers along the C-C bonds (also given in parenthesis). Note the smaller scales for $\text{Au}_{3,4}$.

Figure 9 shows the differences in the total energies, ΔE_0 , of the five clusters with respect to the total energy at their binding site, i.e. top ($\text{Au}_{1,2}$ and Au_4^Y) and bridge for the remaining two.

Note that only Au_2 binds on both the top and bridge position, while the other four clusters have a saddle point at the bridge (Au_1 and Au_4^Y) or top (Au_3 and Au_4^D) position, respectively, i.e. if allowed they relax to their

stable binding site. These transition states define the diffusion barriers of the gold clusters along the C-C bonds. For convenience the diffusion barriers are also explicitly given in Fig. 9. They range from only 4 meV for Au_2 and Au_4^D , making them highly mobile, to 36 meV for the least mobile trimer.

The adsorption energies of all five gold clusters on graphene, cf. Fig. 2 (a), exceed their diffusion barriers by at least one order of magnitude. Hence, while these small gold clusters will rather strongly adsorb onto the graphene sheet, they will easily diffuse even at very low temperatures.

B. Clustering of pre-adsorbed fragments

We modeled the initial clustering processes of gold on graphene in two steps. First, we simulated the formation of a dimer out of two pre-adsorbed gold atoms, cf. Figs 10 and 11. Second, two possible pathways for forming a tetramer, cf. Fig. 12, were explored. At the same time, the formation of a trimer out of a dimer and adatom was studied, too.

In order to simulate the clustering of two pre-adsorbed gold atom, they were initially placed as far away from each other as possible on a 5×5 graphene sheet, i.e. 7.1 Å. This configuration is named position 1 in Figs 10 and 11. Since the total energy of the system decreases only marginally between position 1 and 2, we omitted intermediate steps, cf. Fig. 10.

In the subsequent steps, i.e. position 2 to 6, the second gold atom was brought closer to the fixed one along two C-C bonds, see inset in Fig. 10. For each of the positions 1 - 6 only the x-y-coordinates of the adatoms and one carbon atom at the rim were kept fixed, while z-coordinates of the adatoms and the rest of the graphene sheet could fully relax. In a final step we allowed the system to freely relax from position 6 and without an additional activation barrier it converged to the dimer ground state (position 7). This final structure is identical to the one we found in Sec. III by soft-landing the dimer on graphene, see Fig. 1 (b).

Both, in the gas phase and on graphene, the formation of a gold dimer is exothermic with a gain in total energy per gold atom of $\Delta E_0 = -1.14$ and -1.29 eV, respectively, see Fig. 10. The higher energy gain on graphene is a result of the higher adsorption energy of Au_2 compared to two adatoms, see E_{ads} in Fig. 2 (a). ΔE_0 largely exceeds both the adsorption energy as well as the diffusion barriers of Au_1 /graphene. Thus the driving forces behind the clustering of two pre-adsorbed gold adatoms is the opportunity to lower the total energy of the system by forming strong gold-gold bonds, i.e. the strongly hybridized *d*-states in Fig. 6. At the positions 3 to 6 forces act on the two adatoms that try to pull them towards each other. This attractive, graphene mediated interaction has a maximal range of approximately 4.3 Å, i.e. the Au-Au distance in position 3. At this distance the two

gold atoms are still well separated in the gas phase.

Note that the last two positions represent a dimer that is parallel (position 6) and perpendicular (position 7) to the graphene sheet. Obviously, in the gas phase the total energies have to be identical for position 6 and 7.

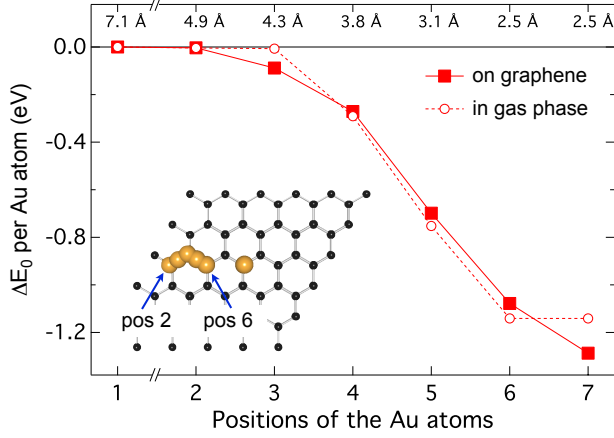


FIG. 10: (Color online) Changes in the total energy ΔE_0 when forming Au_2 /graphene from two pre-adsorbed adatoms (solid symbols) and for the dimer formation in the gas phase (open symbols). The x-y coordinates of the Au adatoms were kept fixed for positions 1-6. The system relaxes without an additional activation barrier from position 6 to 7, the dimer ground state structure (Fig. 2 (b)). The Au-Au distances for the different positions are given on the top axis.

Figure 11 shows the changes in the spin-projected total DOS during the intermediate steps of forming a gold dimer on graphene, cf. position 1 to 7 in Fig. 10. Note that even for the largest possible separation of the two adatoms in the 5×5 super-cell, i.e. 7.1 Å (position 1), there is still an electrostatic interaction between the charged gold atoms, cf. Fig. 1 (a). This can be seen from their 6s-states near the Fermi level that should exactly coincide without any mutual interaction. At a Au-Au distance of 4.9 Å (position 2) the 6s peak splitting becomes more visible. But still the 6s-states below the Fermi level belong solely to the spin-up channel. When the graphene mediated attraction between the adatoms becomes obvious at a distance of 4.3 Å, see ΔE_0 at position 3 in Fig. 10, one of the 6s spins flips, leaving the total system with no total magnetic moments, as we saw above for the closed shell system Au_2 /graphene. Upon further approach of the two gold atoms the two atomic 6s-states form a molecular orbital that moves to lower energies. Finally, it hybridizes with the d_z^2 -states, cf. peaks 4 and 6 in Fig. 6, in the dimer ground state structure (position 7). Meanwhile the unoccupied 6s-states directly above the Fermi level in pos. 3 - 6 move up in energy to finally form peak no. 7 in Fig. 6.

Our next aim was to study the formation of $\text{Au}_{3,4}$ on graphene. We accomplished this by allowing two pre-adsorbed fragments to fully relax from an initial state corresponding to position 6 in Fig. 10. There are two

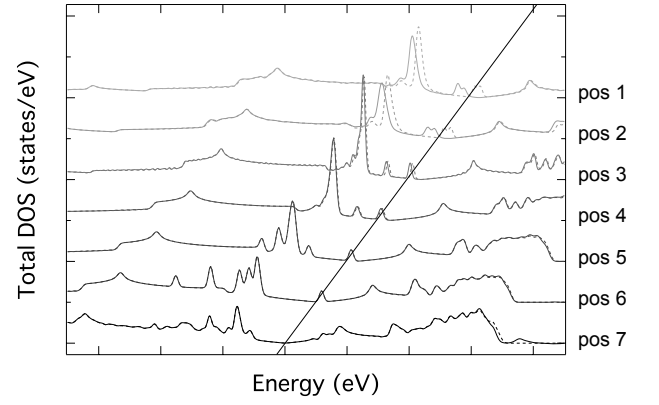


FIG. 11: Changes in total spin-polarized DOS (solid lines spin up; dashed lines spin down) when two pre-adsorbed adatoms come stepwise closer to each other to form Au_2 /graphene, cf. Fig. 10. The diagonal line marks the Fermi energies at the different positions.

different reaction pathways for forming a tetramer, resulting in the two isomers Au_4^D and Au_4^Y , see Figs 1 (d) and (e). In the first reaction pathway two dimers cluster from their perpendicular ground state into the Y shaped tetramer, $2 \cdot \text{Au}_2 \rightarrow \text{Au}_4^Y$. The energy gain per gold atom during this step is $\Delta E_0 = -0.27$ eV, see Fig. 12 (a). Nonetheless, per dimer this energy gain is still bigger than the dimer adsorption energy of -0.47 eV, see Fig. 2 (a), overcompensating the breaking of one Au-C bond to form Au_4^Y /graphene.

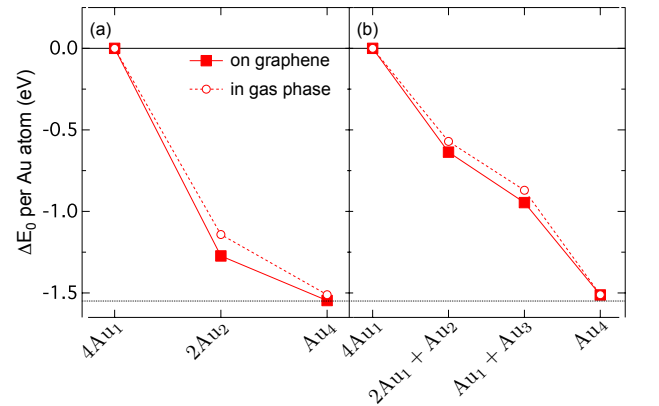


FIG. 12: (Color online) Changes in the total energy ΔE_0 during the formation of Au_4^Y /graphene out of (a) two pre-adsorbed dimers, and (b) Au_4^D out of four adatoms (solid squares). For comparison ΔE_0 for the formation of Au_4^D in the gas phase is shown as well (open circles). The dotted horizontal line marks the highest gain in energy.

The second pathway includes two intermediate steps to form Au_4^D out of four single gold atoms. To begin with, a trimer is formed, $\text{Au}_1 + \text{Au}_2 \rightarrow \text{Au}_3$. Then, by adding yet an adatom, one forms the tetramer: $\text{Au}_1 + \text{Au}_3 \rightarrow \text{Au}_4^D$. The energy gain ΔE_0 during the whole reaction is shown in Fig. 12 (b). This process is exothermic and the

fragments only have to overcome their diffusion barriers, Fig. 9. As for the dimer formation, the energy released by forming the strong Au-Au bonds is the driving force behind the clustering, which is for all steps bigger than the cost of breaking a Au-C bond or overcoming diffusion barriers.

Although we did not explicitly calculate the stepwise movement of the different fragments, as we did in the case of two adatoms, see Fig. 10, we expect a similar behavior due to the high mobility of the pre-adsorbed clusters, see Sec. IV.

A comparison of ΔE_0 in Figs 12 (a) and (b) shows, as mentioned in Sec. III, that $\text{Au}_4^Y/\text{graphene}$ is 137 meV lower in energy than $\text{Au}_4^D/\text{graphene}$. The open symbols in Fig. 12 show the energies of the reaction steps in the gas phase. Since Au_4^D is the gas phase ground state structure, we assumed that both reaction pathways give this structure. The end points in Fig. 12 (b) seem to coincide, i.e. the energy gain by clustering in the gas phase and on graphene appears to be the same. That is actually the case since the adsorption energy of four Au_1 on graphene is -0.4 eV, which is almost identical to E_{ads} of Au_4^D with -0.41 eV.

V. SUMMARY AND CONCLUSIONS

By means of density functional theory, the adsorption of Au_{1-4} clusters on graphene, their mobility and clustering from pre-adsorbed fragments have been studied. This allowed us to explain the initial steps in the experimentally observed formation of bigger gold aggregates on graphene. While Au_{1-3} adsorb similarly on graphene as on graphite, the tetramer turns out to be more peculiar. In the gas phase it has two isomers, the diamond shaped Au_4^D , being the ground state, and the Y shaped Au_4^Y . On graphene Au_4^Y becomes the ground state instead. Although Au_4^Y binds stronger to the substrate and also receives more charge from it than Au_4^D does, it disturbs the graphene sheet substantially less.

The cluster adsorption energies on graphene of all studied clusters range from -0.1 to -0.59 eV and substantially exceed their diffusion barriers, which are 4 to 36 meV,

only. All clusters diffuse along the C-C bonds, since none of them binds to the hollow sites in the centers of the carbon hexagons.

Our detailed analysis of the densities of states shows which states contribute to the strong intracluster bonds, predominantly the 5*d*-states, and which to the chemical bond between gold and carbon, i.e. mostly *s-d_{z2}*-cluster states hybridizing with *p_z*-states of carbon.

The formation of the strong Au-Au bonds is the driving force behind the tendency to form bigger clusters from smaller pre-adsorbed fragments. We studied these processes in detail for the stepwise formation of a dimer out of two pre-adsorbed adatoms, including the evolution of the electronic structure during the clustering. The exothermic reaction has no additional activation barriers apart from the small diffusion barriers of the fragments moving along the C-C bonds. We find the graphene mediated, attractive interaction of two gold adatoms to have a range of approximately 4.3 Å, which is clearly longer than in the gas phase.

Finally, we have also studied the formation of the trimer and tetramers by the reactions $\text{Au}_1 + \text{Au}_2 \rightarrow \text{Au}_3$, $\text{Au}_1 + \text{Au}_3 \rightarrow \text{Au}_4^D$, and $2 \cdot \text{Au}_2 \rightarrow \text{Au}_4^Y$. Both reactions are also activation barrier free. As for the dimer, the energy gained by clustering, i.e. forming Au-Au bonds, exceeds substantially both the Au-C bond energies as well as the diffusion barriers. Note that both tetramer isomers, i.e. $\text{Au}_4^{Y,D}$ are formed on graphene, depending on the actual reaction pathway.

Acknowledgments

This research was supported by the Swedish Energy Agency (Energimyndigheten) and the Swedish Research Council (Vetenskapsrådet). Computation time on the Neolith Cluster at the National Supercomputer Centre in Linköping and on the Akka Cluster at the High Performance Computing Center North in Umeå was granted by the Swedish National Infrastructure for Computing (SNIC). O. E. is grateful to the European Research Council (ERC) for support.

* Electronic address: martin.amft@fysik.uu.se

¹ D. M. Duffy and J. A. Blackman, Surf. Sci. **415**, L1016 (1998).

² G. M. Wang, J. J. BelBruno, S. D. Kenny, and R. Smith, Surf. Sci. **541**, 91 (2003).

³ A. Maiti and A. Ricca, Chem. Phys. Lett. **395**, 7 (2004).

⁴ K. Novoselov, A. Geim, S. Morozov, D. Jiang, M. Grigorieva, S. Dubonos, and A. Firsov, Nature **438**, 197 (2005).

⁵ K. Novoselov, D. Jiang, F. Schedin, T. Booth, V. Khotkevich, S. Morozov, and A. Geim, PNAS **102**, 10451 (2005).

⁶ A. K. Geim and K. S. Novoselov, Nat. Mater. **6**, 183 (2007).

⁷ M. I. Katsnelson, Mater. today **10**, 20 (2007).

⁸ A. H. Castro-Neto, N. M. R. Peres, K. S. Novoselov, and A. K. Geim, Rev. Mod. Phys. **81**, 109 (2009).

⁹ A. K. Geim, Science **324**, 1530 (2009).

¹⁰ F. Schedin, A. K. Geim, S. V. Morozov, E. W. Hill, P. Blake, M. I. Katsnelson, and K. S. Novoselov, Nat. Mater. **6**, 652 (2007).

¹¹ B. Sanyal, O. Eriksson, U. Jansson, and H. Grennberg, Phys. Rev. B **79**, 113409 (2009).

¹² T. O. Wehling, K. S. Novoselov, S. V. Morozov, E. E. Vdovin, M. I. Katsnelson, A. K. Geim, and A. I. Lichtenstein, Nano Lett. **8**, 173 (2008).

¹³ S. Carara, R. Batista, and H. Chacham, Phys. Rev. B **80**,

- 115435 (2009).
- ¹⁴ K. M. McCreary, K. Pi, A. G. Swartz, W. Han, W. Bao, C. N. Lau, F. Guinea, M. I. Katsnelson, and R. K. Kawakami, *Phys. Rev. B* **81**, 115453 (2010).
 - ¹⁵ J. R. Arthur and A. Y. Cho, *Surf. Sci.* **36**, 641 (1973).
 - ¹⁶ E. Ganz, K. Sattler, and J. Clarke, *Surf. Sci.* **219**, 33 (1989).
 - ¹⁷ R. Anton and I. Schneiderreit, *Phys. Rev. B* **58**, 13874 (1998).
 - ¹⁸ G. M. Wang, J. BelBruno, S. D. Kenny, and R. Smith, *Phys. Rev. B* **69**, 195412 (2004).
 - ¹⁹ P. Jensen, X. Blase, and P. Ordejon, *Surf. Sci.* **564**, 173 (2004).
 - ²⁰ G. M. Wang, J. BelBruno, S. D. Kenny, and R. Smith, *Surf. Sci.* **576**, 107 (2005).
 - ²¹ Z. Luo, L. A. Somers, Y. Dan, T. Ly, N. J. Kybert, E. J. Mele, and A. T. C. Johnson, *Nano Lett.* **10**, 777 (2010).
 - ²² P. E. Blöchl, *Phys. Rev. B* **50**, 17953 (1994).
 - ²³ G. Kresse and D. Joubert, *Phys. Rev. B* **59**, 1758 (1999).
 - ²⁴ G. Kresse and J. Furthmüller, *Comput. Mater. Sci.* **6**, 15 (1996).
 - ²⁵ G. Kresse and J. Furthmüller, *Phys. Rev. B* **54**, 11169 (1996).
 - ²⁶ J. P. Perdew, K. Burke, and M. Ernzerhof, *Phys. Rev. Lett.* **77**, 3865 (1996).
 - ²⁷ J. P. Perdew and Y. Wang, *Phys. Rev. B* **45**, 13244 (1992).
 - ²⁸ B. Hammer, L. B. Hansen, and J. K. Nørskov, *Phys. Rev. B* **59**, 7413 (1999).
 - ²⁹ W. Tang, E. Sanville, and G. Henkelman, *J. Phys. Condens. Matter* **21**, 084204 (2009).
 - ³⁰ G. Bravo-Perez, I. Garzon, and O. Novaro, *J. Mol. Struct. Theochem.* **43**, 225 (1999).
 - ³¹ H. Häkkinen and U. Landman, *Phys. Rev. B* **62**, R2287 (2000).
 - ³² H. Grönbeck and W. Andreoni, *Chem. Phys.* **262**, 1 (2000).
 - ³³ M. Amft and N. Skorodumova, *Phys. Rev. B* **81**, 195443 (2010).
 - ³⁴ J. P. Jalkanen, M. Halonen, D. Fernandez-Torre, K. Laasonen, and L. Halonen, *J. Phys. Chem. A* **111**, 12317 (2007).
 - ³⁵ L. Xiao and L. Wang, *Chem. Phys. Lett.* **392**, 452 (2004).
 - ³⁶ N. V. Skorodumova, S. I. Simak, A. E. Kochetov, and B. Johansson, *Phys. Rev. B* **72**, 193413 (2005).
 - ³⁷ A. Grigoriev, N. V. Skorodumova, S. I. Simak, G. Wendin, B. Johansson, and R. Ahuja, *Phys. Rev. Lett.* **97**, 236807 (2006).
 - ³⁸ J. Akola and H. Häkkinen, *Phys. Rev. B* **74**, 165404 (2006).
 - ³⁹ K. T. Chan, J. B. Neaton, and M. L. Cohen, *Phys. Rev. B* **77**, 235430 (2008).
 - ⁴⁰ R. Varns and P. Strange, *J. Phys. Condens. Matter* **20**, 225005 (2008).